Science of the Total Environment 771 (2021) 145306

Contents lists available at ScienceDirect

Science of the Total Environment

journal homepage: www.elsevier.com/locate/scitotenv

Elucidating the quantitative characterization of atmospheric oxidation capacity in Beijing, China

Zirui Liu [a], Yuesi Wang [a,b,*], Bo Hu [a], Keding Lu [c], Guiqian Tang [a], Dongsheng Ji [a], Xinping Yang [c], Wenkang Gao [a], Yuzhu Xie [a], Jingyun Liu [a,d], Dan Yao [a], Yuan Yang [a], Yuanhang Zhang [c]

[a] State Key Laboratory of Atmospheric Boundary Layer Physics and Atmospheric Chemistry (LAPC), Institute of Atmospheric Physics, Chinese Academy of Sciences, Beijing 100029, China
[b] Center for Excellence in Regional Atmospheric Environment, Institute of Urban Environment, Chinese Academy of Sciences, Xiamen, Fujian 361021, China
[c] State Key Joint Laboratory or Environmental Simulation and Pollution Control, College of Environmental Sciences and Engineering, Peking University, Beijing, China
[d] Department of Environmental Science and Engineering, Beijing University of Chemical Technology, Beijing 100029, China

HIGHLIGHTS

- Newly developed indexes were used to elucidate the atmospheric oxidation capacity (AOC).
- Well-defined seasonal and diurnal patterns of AOC were found in urban and suburban Beijing.
- AOC was dominated by oxidation of CO and alkenes in summer and of CO and NO_2 in winter.
- The dominate contributor to AOC was OH and ozone during the daytime and nighttime, respectively.
- The heterogeneous oxidation processes contributed substantially to the underestimation of AOC.

GRAPHICAL ABSTRACT

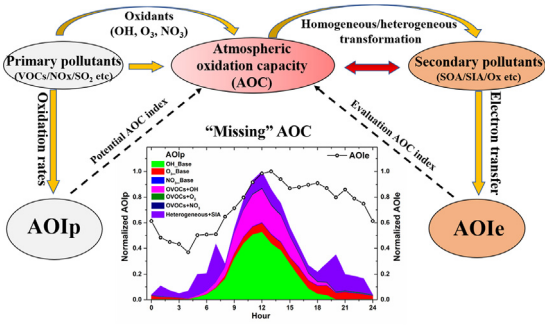

Quantitative characterization of atmospheric oxidation capacity

ARTICLE INFO

Article history:
Received 18 November 2020
Received in revised form 12 January 2021
Accepted 16 January 2021
Available online 22 January 2021

Editor: Jianmin Chen

Keywords:
AOC
Electron transfer reaction
Oxidation rates
Missing AOC mechanism

ABSTRACT

The atmospheric oxidizing capacity (AOC) is the essential driving force of tropospheric chemistry, but its quantitative representation remains limited. This study presents the detailed evaluation of AOC in the megacity of Beijing based on newly developed indexes that represent the estimated oxidative capacity from the prospective of oxidation products (AOIe) and the potential oxidative capacity considering the oxidation rates of major reactants by oxidants (AOIp). A comprehensive suite of data taken from summer and winter field campaigns were used to create these two indexes and in the calculation of AOC. The AOC showed a clear seasonal pattern, with stronger intensity in summer compared to winter. The gaseous-phase oxidation products (O_3 and NO_2) dominated AOIe (~80%) during summertime at both sites, while the contribution of particle-phase oxidation products (sulfate, nitrate, and secondary organic aerosol) to AOIe increased in winter (~30%). As for AOIp in summer, the dominant contributor was alkenes (31.0%, urban) and CO (38.5%, suburban), whereas CO and NO_2 dominated AOIp at both urban (68.8%) and suburban (61.0%) sites during wintertime. As expected, the dominant oxidant contributor to AOIp during the daytime was OH, while O_3 was the second most important oxidant at both sites. The diurnal variations of normalized AOIe and AOIp were examined, revealing that they share the same daytime peak but showed significant bias during the nighttime. To explore the possible deviation in sources between AOIe and AOIp, a constrained photochemical box model and a constrained multiphase chemical box model were used to evaluate AOC budgets and their source apportionment. Our results suggest that unmeasured OVOC

* Corresponding author at: State Key Laboratory of Atmospheric Boundary Layer Physics and Atmospheric Chemistry (LAPC), Institute of Atmospheric Physics, Chinese Academy of Sciences, Beijing 100029, China.
E-mail address: wys@mail.iap.ac.cn (Y. Wang).

https://doi.org/10.1016/j.scitotenv.2021.145306

(oxygenated volatile organic compound) species and missed heterogeneous oxidation processes in the calculation of AOIp contributed substantially to the underestimation of AOC by this index, which should be taken into consideration in future studies of AOC.

1. Introduction

Poor air quality due to unsustainable growth of urban areas affects millions of people worldwide, and is one of the major threats to human health in and downwind of urban areas. With the rapid development of economies and the intensification of urbanization, economically developed regions in eastern China have experienced severe air pollution in recent decades (Chan and Yao, 2008), especially the North China plain region where an unprecedented long-lasting heavy haze pollution episode occurred in January 2013 (Wang et al., 2014a,b; M. Wang et al., 2014), causing more than 600 premature deaths in the Beijing area and leading to economic losses that amounted to 0.08% of the GDP of Beijing that year (Gao et al., 2015). Since then, the toughest-ever "Air Pollution Prevention and Control Action Plan" has been implemented by the State Council of China to improve the air quality nationwide. Subsequently, in the following five years (2013–2017), a reduction of 25% for $PM_{2.5}$ was found in the Beijing–Tianjin–Hebei region, and a similar decreasing trend of $PM_{2.5}$ was also observed in other developed regions of China (Zhang et al., 2019). However, surface ozone (O_3) concentrations showed increasing trends in developed regions from 2013 to 2017 (Wang et al., 2020), which is the only substance among six air quality indexes that has increased during the last five years, and the increased trend of surface ozone was reported to be caused by the decrease in $PM_{2.5}$ which slowing down the sink of hydroperoxy radicals and thus speeding up ozone production (K. Li et al., 2019). In addition, the nitrate component of $PM_{2.5}$ has not shown a consistent decrease, despite nationwide reduction in the emissions of nitrogen oxides (Wang et al., 2019); fine particulate nitrate in winter in Beijing has even shown no decrease, despite a 43% reduction in emissions of nitrogen oxides (NOx) (Gao et al., 2020). These results indicate a nonlinear relationship between primary and secondary pollutants, which may be associated with the enhanced oxidizing capacity in urban environments.

The atmospheric oxidation capacity (AOC) is the essential driving force of atmospheric chemistry in forming complex air pollution (Li et al., 2018), which determines the removal rate of trace gases and also the production rates of secondary pollutants (Prinn, 2003). The processes and rates of species being oxidized in the atmosphere thus constitute the key factors to quantify AOC. Several studies have been carried out to quantify the atmospheric oxidation processes, including: field observation of key oxidizing species and their precursors in urban and suburban environments (Elshorbany et al., 2009; Xue et al., 2016; Lu et al., 2012); laboratory dynamics studies on the conversion of various precursors to the contribution of the free radical sources (George et al., 2005; Stemmler et al., 2006, 2007); and numerical model studies to quantitatively evaluate the oxidation of trace gases in urban environments (L. Liu et al., 2019). Currently, the term "oxidation capacity" is defined as the sum of the respective oxidation rates of the molecules (VOCs, CO, CH_4, etc.) by the main oxidant (OH, O_3, NO_3, etc.) (Geyer et al., 2001), and these oxidation processes are described in atmospheric chemical reaction mechanisms such as the RACM (Regional Atmospheric Chemistry Mechanism) and MCM (Master Chemical Mechanism). However, recent modelling studies have shown that traditional gas-phase chemistry in the RACM or MCM cannot explain the rapid secondary aerosol production observed during winter haze in China (Zheng et al., 2015; Zhang et al., 2015; Shao et al., 2019), suggesting the existence of missing AOC mechanisms in the formation of secondary aerosol. In addition, developed countries have not eliminated the O_3 pollution problem, despite strict controls on NOx and VOC emissions (Parrish et al., 2011), indicating the current control strategy has lost sight of O_3 pollution, possibly due to inadequate understanding of the AOC. Therefore, a deeper understanding the AOC is the priority before any efficient pollution mitigation can take place.

The present study focuses on the quantitative characterization of AOC in the polluted atmosphere of Beijing, and constitutes the first detailed evaluation of AOC using newly developed AOC indexes through analyzing the comprehensive observation of gaseous and particulate chemical composition data obtained from intensive field campaigns. In addition, a constrained photochemical box model based on the MCM and a constrained multiphase chemical box model (RACM-CAPRAM) were used to model the key primary species being oxidized and the important formation pathways of their secondary products, which help to evaluate AOC budgets and their source apportionment and thus provide better understanding on the missing sources of AOC from current photochemical mechanisms in the highly polluted urban environment.

2. Methods

2.1. Experiments

The field measurements were performed in parallel at an urban site in the downtown area of Beijing and a suburban site approximately 50 km southeast of the central Beijing. The urban station was located in the northern part of Beijing, which was well-known as the IAP site (116° 22′E, 39° 58′N, 45 m above sea level) for long-term monitoring of urban air quality since 2004 (Liu et al., 2015). The suburban site was located at Xianghe (116° 95′E, 39° 76′N, 25 m above sea level), which is an air monitoring station operated by the Institute of Atmospheric Physics, Chinese Academy of Sciences. The Xianghe site is surrounded by residential areas and agricultural land, and has been used as a typical suburban site to evaluate the influence of polluted plumes transported from urban Beijing and other megacities of North China Plain in previous studies (Liu et al., 2018). In the present study, a 3-month measurement campaign was carried out from 1 June to 15 July 2018 and from 1 December 2018 to 15 January 2019, which covered the summer and winter seasons, respectively.

The comprehensive observation of gaseous pollutants, particulate chemical compositions and meteorological parameters using state-of-the-art instruments were conducted at the urban and suburban sites. Detailed description about these instruments and their calibration procedures have been provided in our previous studies (Liu et al., 2016; L. Liu et al., 2019; Z. Liu et al., 2019; Yang et al., 2019; Li et al., 2020a). Briefly, the gaseous species (O_3, NO/NO_2/NOx, CO, SO_2) were measured using the commercial instruments (Model series I, Thermo Scientific, USA), while a tapered element oscillating microbalance (TEOM 1405-DF, Thermo Scientific, USA) was used to measure the $PM_{2.5}$ mass concentrations. The ambient VOC concentrations were analyzed on-line using a gas chromatograph instrument (7820A, Agilent Technologies, Santa Clara, CA, USA) equipped with an MS and an FID (5977E, Agilent Technology, Santa Clara, CA, USA) (Wang et al., 2014a,b; M. Wang et al., 2014), and a total of 100 VOC species were quantified, including 28 alkanes, 12 akenes, 1 alkyne (acetylene), 16 aromatics, 12 OVOCs (oxygenated VOCs), and 31 haloalkanes. The detailed compounds that used in this study were summarized in Table S1. The chemical compositions of nonrefractory submicron particles (NR-PM_1) were measured by a high-resolution time-of-flight aerosol mass spectrometer (HR-ToF-AMS, Aerodye Inc., USA). The photolysis rates of $j(O^1D)$, $j(NO_2)$ and $j(NO_3)$ were calculated using the actinic radiation flux values which converted

from the irradiance measured with a spectroradiometer (DTMC300, Bentham, England). Meteorological parameters, including temperature, humidity, pressure, solar radiation, wind speed, and wind direction were monitored by automatic meteorological monitoring instruments (Milos520, Vaisala, Finland).

2.2. Evaluation of AOC by index methods

At present, there is no uniform, globally accepted quantitative index to characterize the AOC. The present study introduces two kinds of AOC index: one is the evaluation index (AOIe), which estimates the AOC from the perspective of electron transfer during the formation of atmospheric oxidation products (secondary pollutants); and the other is the potential index (AOIp), which is calculated as the sum of oxidation rates of major reductants by the principal oxidants. Detailed descriptions of these two AOC indexes are provided below.

2.2.1. Evaluation index of AOC (AOIe)

Anthropogenically emitted reducing pollutants, after reacting with various oxidants in the atmosphere, are converted from low-valent primary pollutants to high-valent secondary pollutants. The essence is that electrons are transferred from the reducing agent to the oxidizing agent, or electron hopping from one moiety to another. Electron transfer reaction is an important elementary chemical reaction during the oxidation–reduction reaction of air pollutants. Based on this theory, this study seeks to qualify the AOC by calculating the mole number of transferred electrons based on the oxidation products such as the major gaseous-phase products and major particle-phase products. According to the definition of AOIe, it can be calculated by Eq. (1):

$$AOI_e = f_{e1(NOx\,to\,NO_3^-)} + f_{e2(SO_2\,to\,SO_4^{1-})} + f_{e3(VOCs\,to\,SOA)} + f_{e4(NO\,to\,NO_2)} + f_{e5(O\,to\,O_3)}, \quad (1)$$

where f_{e1-5} denote the molar number concentrations of electrons during the oxidation processes of NOx, SO_2, VOCs and the formation of O_3, respectively. The molar number concentrations of electrons were calculated from the difference of valence between the reductants and the oxidation products. For example, the valence of elemental sulfur in the reductant (SO_2) and oxidation product (SO_4^{2-}) is positive tetravalent (S(IV)) and positive hexavalent (S(VI)), respectively. Then, the molar number concentration of electrons for f_{e2} is calculated from the molar mass concentration of SO_4^{2-}, multiplied by two, which denotes the change in valence of elemental sulfur from positive tetravalent to positive hexavalent. The amount of electron transfer during the oxidation of NOx to nitrate was considered. Note that the change in valence of elemental nitrogen should be divided into two parts when considering the NO_3^- formation: one is from positive divalent (NO, N(II)) to positive pentavalent (NO_3^-, N(VI)), and the other is from positive tetravalent (NO_2, N(IV)) to positive pentavalent (NO_3^-, N(VI)). It should be noted that NOx can be also oxidized to other products, such as PANs, organic nitrate aerosol, etc. These transformation processes were not considered in this study which may underestimate AOIe. However, as the concentration of these products is much lower than the nitrate concentration, this kind of underestimation should be insignificant. In addition, due to the large variety of VOCs and the complex structure of secondary organic aerosol (SOA), it is not yet possible to accurately understand the conversion of all VOC species to SOA in the atmosphere, making it difficult to quantify the total number of electrons transferred in the SOA formation processes. Instead, we use the oxygen content in SOA as a proxy to characterize the total number of electrons since the majority of primary VOC species emitted from anthropogenic and natural sources were oxygen-free, which means the electrons transferred in the SOA formation could be simply equal to the change of oxygen valence in the SOA. The oxygen content in SOA was calculated based on the oxygen-to-carbon (O/C) ratios in organic aerosols measured by the HR-ToF-AMS and the SOA concentrations resolved from organic aerosol source appointment (Li et al., 2020b), and the molar number concentrations of electrons during the oxidation processes of VOCs could be calculated by Eq. (2):

$$f_{e3(VOCs\,to\,SOA)} = SOA \times \left(\frac{O/C}{1+O/C}\right) \times 2. \quad (2)$$

2.2.2. Potential index of AOC (AOIp)

The potential oxidative capacity of the atmosphere (AOIp) is determined by quantifying the loss rates of trace gaseous pollutants via reactions with the main atmospheric oxidants (Elshorbany et al., 2009; Xue et al., 2016), the quantitation of which can be calculated by Eq. (3):

$$AOI_p = \sum_{j=1}^{m}\left\{[C_j] \times \sum_{i=1}^{n} k_{ij}[X_i]\right\}, \quad (3)$$

In this study, C_j denotes the primary pollutants of VOCs, CO, NO*x* and SO_2; X_i denotes the oxidants of OH, O_3 and NO_3; and k_{ij} is the bimolecular rate constant for the reaction of C_j with X_i. The information on the primary pollutants included in the AOIp calculation and their reaction rates with oxidants is presented in Table S1. Note than the target VOCs used in calculating AOIp were selected that registered in MCM3.3.1. In addition, the oxidants of OH and NO_3 radicals were estimated from parameterization methods introduced by previous studies (Ehhalt and Rohrer, 2000; Yuan et al., 2013; Tham et al., 2018), and a brief description of the calculation processes were provided in the supporting information. The calculated OH and NO_3 radical showed similar diurnal variations as those modelled by a box model constrained by observations (Fig. S2a). In addition, the calculated OH in this study was on average 28.4% lower and 94.3% higher than the modelled values during the summer and winter campaigns, in accordance with the uncertainties reported by Zheng et al. (2011). Note that the calculated OH was closer to the measured OH than the modelled ones during the winter campaign in Beijing (Fig. S3). OH mixing ratio was measured using a laser induced fluorescence (LIF) instrument during a 13-day field campaign conducted at the campus of Peking University (Lu et al., 2018). Thus, the parameterization methods were used to calculate OH and NO_3 radical concentrations in this study, as the measured values was unavailable for the whole campaign for both sites and the modelled values seem to be much underestimated.

3. Results and discussion

3.1. Overview of the observation periods

The measured time series of major gaseous pollutants and meteorological parameters at the urban and suburban sites during the campaigns from 1 June to 15 July 2018 and from 1 December 2018 to 15 January 2019 are depicted in Fig. 1. During the summer campaign, the average temperature and relative humidity were 27.9 ± 4.6(26.8 ± 4.9)°C and 49.8 ± 21.5(68.7 ± 22.6)%, respectively, while the average concentrations of SO_2, CO, NO_2, NO and O_3 were 0.85 ± 0.91(2.78 ± 1.20) ppb, 1.36 ± 0.36(1.08 ± 0.50) ppm, 18.9 ± 9.8(15.2 ± 7.8) ppb, 3.8 ± 4.8(2.7 ± 5.0) ppb, 48.9 ± 31.6(54.1 ± 35.7) ppb, for the urban (suburban) sites. The average $PM_{2.5}$ concentration during the summer campaign was 49.4 ± 30.8 and 40.0 ± 21.2 μg m^{-3} for the urban and suburban sites, respectively, with days of good air quality (daily $PM_{2.5}$ < 75 μg m^{-3} according to the Ambient Air Quality Standard (GB3095-2012) of China) accounting for 84.4% and 100% for the urban and suburban sites, suggesting good air quality represented by the fine particles during the summer campaign. However, high-O_3 pollution days were frequently observed, with 17 and 29 days exceeding the Class 2 standard for O_3 in the Ambient Air Quality Standards of China (GB 3095-2012, hourly O_3 > 93 ppb). All the gaseous pollutants except O_3 were largely increased during the winter campaign, with the average

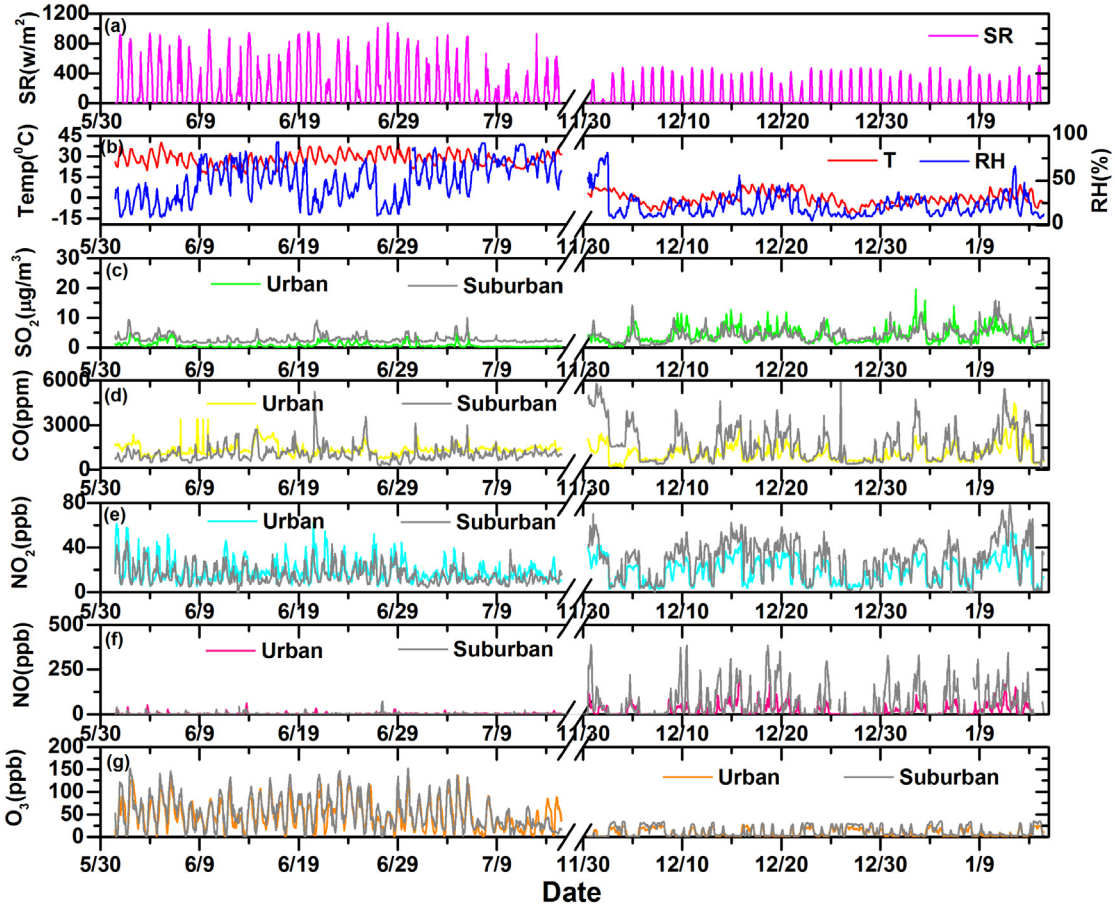

Fig. 1. Time series of major pollutant mixing ratios and meteorological parameters at the urban and suburban sites in Beijing during the summer (1 June to 15 July 2018) and winter (1 December 2018 to 15 January 2019) campaigns. The meteorological data was only for the urban site.

concentrations of SO_2, CO, NO_2 and NO being 4.12 ± 2.68(4.24 ± 2.38) ppb, 1.07 ± 0.56(1.70 ± 1.22) ppm, 19.1 ± 11.2(29.1 ± 17.0) ppb, 22.5 ± 31.1(68.1 ± 85.5) ppb, for the urban(suburban) sites. In comparison, the average O_3 concentrations decreased to 9.2 ± 8.2 and 12.4 ± 10.9 ppb. Note that the average $PM_{2.5}$ concentration during the winter campaign also increased, especially for the suburban site, which were 52.2 ± 55.2 and 57.1 ± 54.6 μg m^{-3} for the urban and suburban sites, suggesting enhanced fossil fuel combustion for domestic heating in winter in Beijing. The comparable concentration in SO_2 but much higher concentration in NOx for the suburban site may suggest different kinds of fossil fuels used for heating between the urban and suburban areas of Beijing.

The difference in the air pollution conditions between the urban and suburban sites was also reflected by the chemical composition of submicron particles. Table 1 lists the average concentrations of major chemical species in PM_1. It clearly shows that the average concentrations of the five species (organics, NO_3^-, SO_4^{2-}, NH_4^+ and Cl^-) during the summer campaign were higher at the suburban site than those at the urban site, especially for nitrate, which was more than two times higher at the suburban site. A similar phenomenon was also observed during the winter campaign, except the nitrate showed slightly higher values at the urban site. Different from the results of the particulate chemical components, the VOC species were higher at the urban site during the summer campaign. As shown in Table 1, the largest difference was for OVOCs, being 10.5 ± 3.3 ppb and 3.4 ± 1.4 ppb at the urban and suburban sites, respectively. During the winter campaign, however, the VOC species were much higher at the suburban site, except for the OVOCs. Such a difference in the gaseous pollutants and particle chemical compositions will result in different atmospheric chemical processes between the urban and suburban sites, such as the loss rates of CO, SO_2, NO_2 and VOCs via reactions with OH, O_3 and NO_3, which are representative of the AOC as discussed in detail in the following sections.

3.2. Atmospheric oxidative capacity

In this study, two kinds of atmospheric oxidation indexes are introduced to quantify the AOC during summer and winter in Beijing, which

Table 1
Summary of the average pollutant concentrations, meteorological parameters and AOC index values for the summer and winter campaigns.

Parameters	Urban		Suburban	
	Summer	Winter	Summer	Winter
$PM_{2.5}$ (μg m^{-3})	49.4 ± 30.8	52.2 ± 55.2	40.0 ± 21.2	57.1 ± 54.6
Org. (μg m^{-3})	7.8 ± 4.0	10.7 ± 11.9	8.6 ± 5.1	19.2 ± 18.2
NO_3^- (μg m^{-3})	2.9 ± 5.4	6.2 ± 11.2	7.6 ± 6.6	5.7 ± 6.8
SO_4^{2-} (μg m^{-3})	4.8 ± 3.3	3.1 ± 6.4	6.0 ± 3.5	4.2 ± 6.1
NH_4^+ (μg m^{-3})	2.3 ± 2.2	3.0 ± 5.1	5.5 ± 3.5	3.8 ± 4.5
Cl^- (μg m^{-3})	0.02 ± 0.03	0.37 ± 0.50	0.09 ± 0.08	0.65 ± 0.69
Alkanes (ppb)	17.8 ± 6.8	21.0 ± 14.1	13.5 ± 8.6	33.1 ± 36.6
Alkenes (ppb)	3.7 ± 1.1	8.1 ± 6.9	2.8 ± 2.3	11.6 ± 13.5
Aromatics (ppb)	4.9 ± 1.9	4.7 ± 3.5	3.7 ± 4.7	10.2 ± 14.8
OVOCs (ppb)	10.5 ± 3.3	4.2 ± 5.1	3.6 ± 1.2	3.4 ± 4.9
Haloalkanes (ppb)	5.2 ± 2.1	3.2 ± 2.7	4.7 ± 3.7	9.1 ± 15.4
$JO^1D \times 10^6$ (s^{-1})	10.6 ± 9.3	4.4 ± 2.8	10.8 ± 9.7	1.4 ± 1.8
$JNO_2 \times 10^3$ (s^{-1})	3.1 ± 1.6	3.0 ± 1.0	3.5 ± 1.7	1.4 ± 1.6
AOle (μmol m^{-3})	4.76 ± 1.32	2.81 ± 1.61	4.77 ± 1.64	4.16 ± 2.11
AOlp $\times 10^7$ (cm^{-3} s^{-1})	2.81 ± 3.42	0.51 ± 0.75	2.71 ± 3.47	0.31 ± 0.54

represent the estimated capacity of atmospheric oxidation (AOIe) and the potential capacity of atmospheric oxidation (AOIp). The seasonal variations and diurnal patterns of these two AOC indexes are discussed in the following subsections.

3.2.1. Estimated oxidative capacity of the atmosphere (AOIe)

The estimated oxidative capacity of the atmosphere was estimated by quantifying the electron transfer during the formation of gaseous-phase oxidation products (O_3 and NO_2) and particle-phase oxidation products (nitrate, sulfate and SOA). During the summer campaign, the 24-hour average AOIe value at the urban site was 4.76 ± 1.32 μmol m^{-3}, and a comparable value of 4.77 ± 1.64 μmol m^{-3} was observed for the suburban site. At the urban site, the average oxidation capacity of gaseous-phase oxidation products (AOIe_G) and particle-phase oxidation products (AOIe_P) was 4.16 ± 1.22 μmol m^{-3} and 0.60 ± 0.31 μmol m^{-3}, representing 87.4% and 12.6% of the total oxidation capacity, respectively. The average value of AOIe_G and AOIe_P at the suburban site was 3.84 ± 1.36 μmol m^{-3} and 0.93 ± 0.47 μmol m^{-3}, accounting for 80.4% and 19.6% of the total oxidation capacity, respectively. Clearly, the gaseous-phase oxidation products dominated the AOC during summertime in both the urban and suburban area of Beijing. During the winter campaign, the average value of AOIe decreased to 2.81 ± 1.61 μmol m^{-3} at the urban site, which could mainly be attributed to the large decrease in AOIe_G (1.95 ± 0.64 μmol m^{-3}), while the average AOIe_P increased substantially to 0.86 ± 1.04 μmol m^{-3}. Note that the winter AOIe at the suburban site remained at a similar level (4.16 ± 2.11 μmol m^{-3}) to that in the summer owing to the insignificant decrease in AOIe_G (2.95 ± 0.99 μmol m^{-3}) and large increase in AOI_P (1.21 ± 1.23 μmol m^{-3}). Although the winter AOC was still mainly contributed by the gaseous-phase oxidation products (~70%), particle-phase oxidation products also played an important role in the winter AOC of Beijing. The contributions of individual oxidation products to the total AOIe are further discussed for the urban and suburban sites. As shown in Fig. 2a and b, the majority of AOIe was contributed by O_3 at both sites, accounting for 52.1% and 54.2% of the total AOIe. The second largest contributor for summer AOIe was NO_2, which showed a higher contribution at the urban site (35.3%) than at the suburban site (26.2%). In comparison, the contribution from secondary aerosol was relatively small. During the winter campaign, the NO_2 became the dominant contributor to the AOIe at both sites, accounting for 54.4% and 58.2% at the urban and suburban sites, respectively. In addition, the second largest contributor was O_3 at the urban site, while it was SOA at the suburban site, suggesting particle-phase oxidation products play the more important role in AOC at the suburban site.

The diurnal variation patterns of AOIe were examined and the results are shown in Fig. 3. During the summer campaign, the lowest value of AOIe (3.64 μmol m^{-3}) appeared at 03:00 at the urban site. Then, it rose rapidly and reached its highest value (5.77 μmol m^{-3}) at about 12:00, after which AOIe decreased slightly but still maintained at a high level for 6 h. After sunset, AOIe decreased continually until reached its lowest value on the second day. Note that the diurnal variation of AOIe was mainly contributed by the gaseous-phase oxidation products, which shared a similar pattern with the total AOIe, while the particle-phase oxidation products showed an almost flat diurnal variation pattern and contributed negligibly to the total AOIe (Fig. 3a). Among the gaseous-phase oxidation products, O_3 was clearly the dominant oxidant during the daytime, contributing by a maximum of 4.06 μmol m^{-3} (71.6%) to the total AOIe at about 13:00. The NO_2 contribution to AOIe during daytime ranged from 17% to 58%, while it reached >67% during the nighttime (Fig. 4a). Similar diurnal variation patterns of AOIe were also observed for the suburban site during summertime, except that the lowest value (3.63 μmol m^{-3}) appeared at 04:00—an hour later than that in the urban site; while the highest value (5.90 μmol m^{-3}) also appeared at 12:00. In addition, a high level of AOIe during the afternoon (12:00–16:00) was more visible at the suburban site. Similarly, the diurnal variation of AOIe at the suburban site also mainly derived from the gaseous-phase oxidation products, and O_3 dominated the daytime AOIe with a maximum value of 4.31 μmol m^{-3} (73.5%) appearing at about 13:00 (Fig. 4c). However, the particle-phase oxidation products at the suburban site showed a

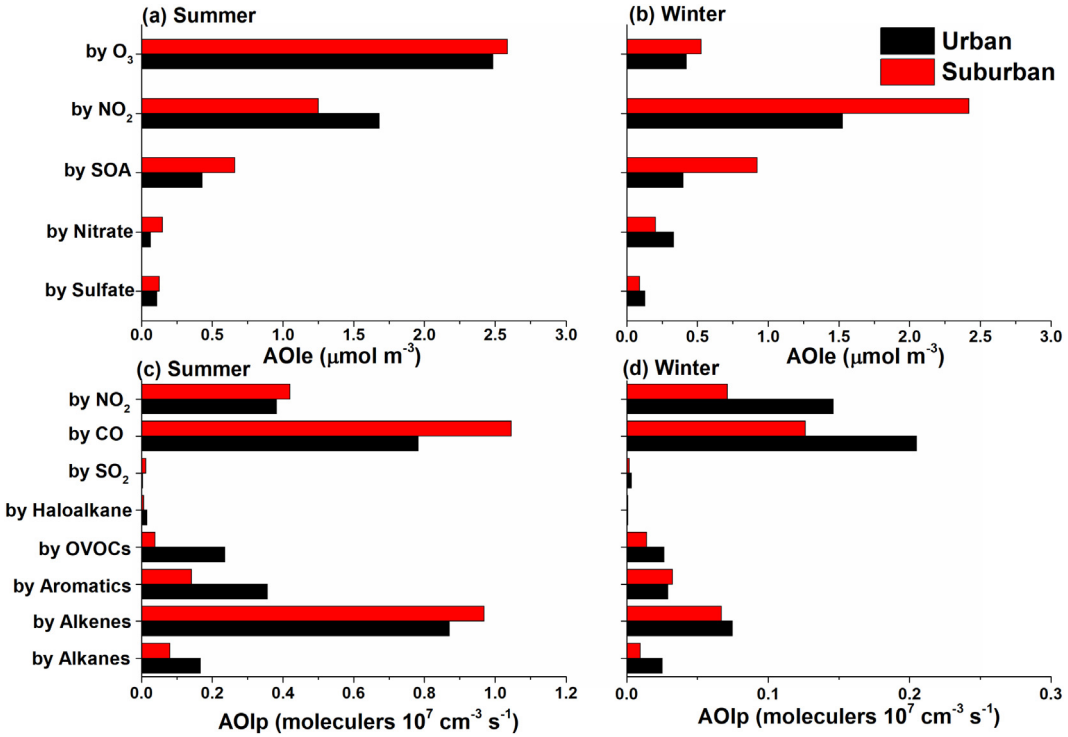

Fig. 2. Contributions of (a, b) major oxidation products to AOIe and (c, d) the major reductants to AOIp at the urban and suburban sites in Beijing during the summer and winter campaigns.

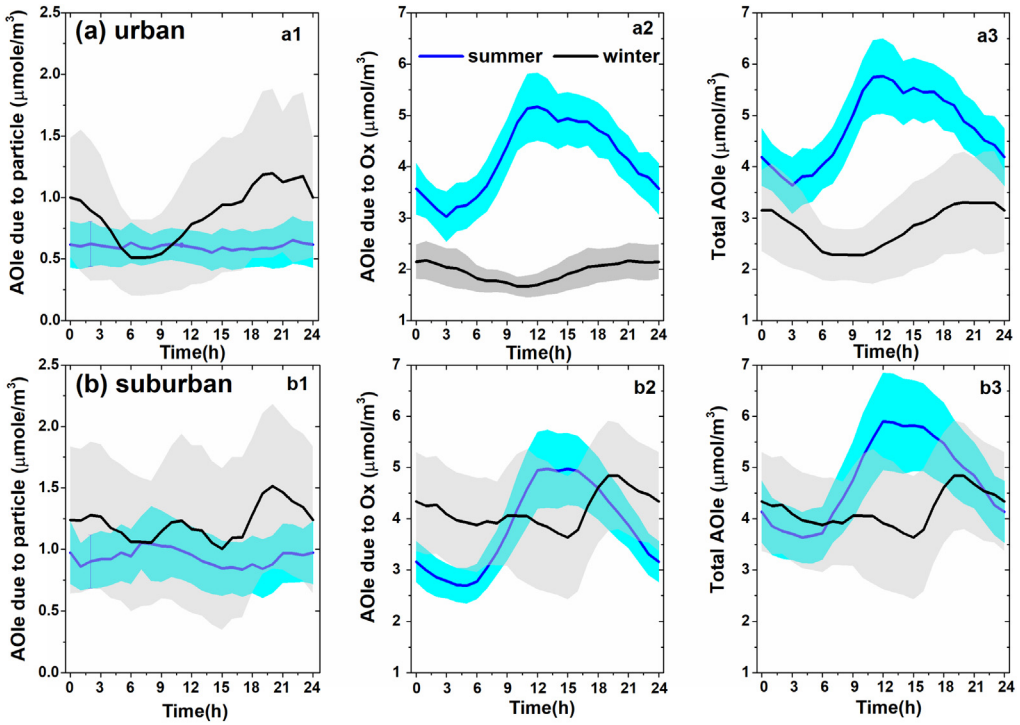

Fig. 3. Diurnal variation of AOIe due to particle-phase oxidation products (AOIe_P for a1 and b1), AOIe due to the gaseous phase oxidation products (AOIe_G for a2 and b2), and the total AOIe (a3 and b3) at the urban and suburban sites in Beijing during the summer and winter campaigns.

more obvious diurnal pattern compared to those at the urban site (Fig. 3b), with a higher contribution from nitrate during the nighttime. These results indicate the atmospheric oxidation condition in the suburban area might be more favorable for secondary aerosol formation during summertime.

The diurnal patterns of AOIe in the winter campaign were totally different from those in summer. For the urban site, the lowest value of AOIe (2.45 μmol m^{-3}) appeared at 07:00 and remained almost stable until 10:00, before it then began to increase linearly to reach its highest value (3.82 μmol m^{-3}) at about 20:00. Note that the high level of AOIe

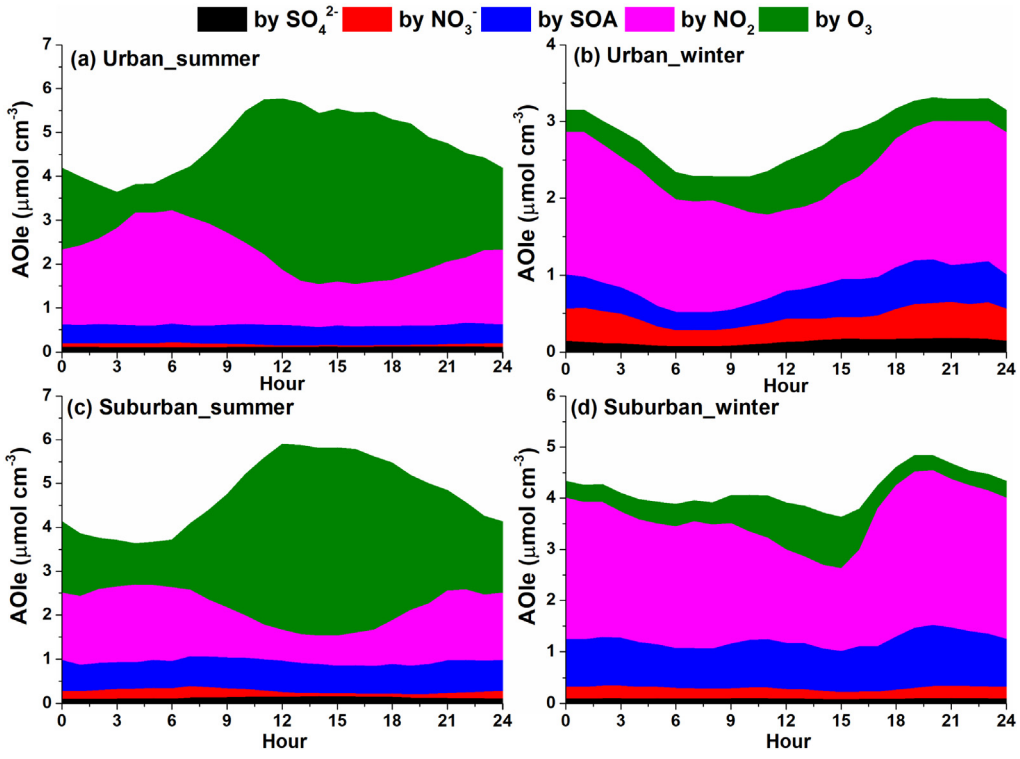

Fig. 4. Diurnal variation of AOIe and the contributions of major oxidation products at the (a) urban and (b) suburban sites in Beijing during the summer and winter campaigns.

during the afternoon disappeared in winter and higher values of AOIe were observed during the nighttime, which was the reverse to that in summer. In addition, NO_2 became the dominant oxidant, and the maximum value of 1.88 μmol m^{-3} (59.7%) was observed at about 01:00 (Fig. 4b). Furthermore, distinct diurnal variation of winter AOIe_P was observed, with the contribution to the total AOIe reaching a maximum of 36.3% during the nighttime. A different diurnal pattern of winter AOIe was observed at the suburban site. As shown in Fig. 3b, AOIe decreased continually from 0:00 to 15:00, then increased significantly from 3.63 μmol m^{-3} at 15:00 to 4.87 μmol m^{-3} at 20:00. Interestingly, the diurnal variation of AOIe_G shared a similar pattern with that of AOIe_P at the suburban site. Specifically, NO_2 dominated the gaseous-phase oxidation products while SOA dominated the particle-phase oxidation products and their contributions both increased during the nighttime (Fig. 4d). This may suggest similar formation processes at the suburban site during wintertime.

3.2.2. Potential oxidative capacity of the atmosphere (AOIp)

During the summer campaign, the calculated AOIp showed comparable values at the urban and suburban sites, with an 24-hour averaged value of 2.81×10^7 and 2.71×10^7 molecules cm^{-3} s^{-1}, respectively, which are 10 times higher than those (2.65×10^6 molecules cm^{-3} s^{-1}) observed in Berlin, Germany (Geyer et al., 2001); but still lower than those (4.14×10^7 molecules cm^{-3} s^{-1}) reported in Santiago, Chile (Elshorbany et al., 2009). In addition, the maximum hourly value of AOIp was slightly higher in the suburban (1.71×10^8 molecules cm^{-3} s^{-1}) than the urban area (1.49×10^8 molecules cm^{-3} s^{-1}), and these values are largely higher than the maximum value of AOC (1.0×10^8 molecules cm^{-3} s^{-1}) observed in Shanghai during the same period as the present study (Zhu et al., 2020), suggesting the stronger AOC in the northern megacities. Note that two more loss rates of SO_2 and NO_2 via reactions with OH radical were included in AOIp calculation compared with previous studies (Geyer et al., 2001; Elshorbany et al., 2009), which would be more representable for qualifying the AOC in polluted urban atmosphere, considering their contribution were above 10% of the total AOC (Fig. 2). During wintertime, significant reductions of AOC were observed at both sites, with an average AOIp of 0.51×10^7 and 0.31×10^7 molecules cm^{-3} s^{-1}, respectively, consistent with a previous study on the seasonal pattern of AOC at other urban locales (Li et al., 2018).

As shown in Fig. 2c, the major reductants that contributed to the total AOIp during summertime were alkenes (31.0%) at the urban site and CO (38.5%) in the suburban site. In addition, CO and alkenes were also the second largest contributors at the urban (28.6%) and suburban (35.7%) sites, respectively. The third largest contributor was NO_2 at both sites, which accounted for more than 13% of AOIp. Note that aromatics and the measured 12 OVOCs also contributed substantially to the summer AOIp at the urban site (~20%), while their contribution was negligible at the suburban site. During the winter campaign, AOIp was mainly contributed by CO, NO_2 and alkenes at both sites (Fig. 2d), accounting for 83.4% (urban) and 81.8% (suburban) of the total AOIp. In addition, aromatics also contributed considerably to the AOIp at both sites (~10%) during wintertime.

The diurnal variation patterns of AOIp due to three major oxidants (OH, O_3 and NO_3) and the total AOIp for the urban and suburban sites are presented in Fig. 5. During the summer campaign, AOIp showed a unimodal diurnal pattern at both the urban and suburban sites, with peak values of 8.85×10^7 and 8.54×10^7 molecule cm^{-3} s^{-1}, respectively. Note that the peak value of AOIp at the urban site appeared at 11:00, while that at the suburban site was 2 h later at 13:00, with a peak value of 3.5% lower than that at the urban site, suggesting a slightly stronger AOC for the urban site during the summertime. The average oxidation capacity of OH, O_3 and NO_3 radicals through the entire day at the urban site during summertime was 2.28×10^7, 4.87×10^6 and 4.15×10^5 molecule cm^{-3} s^{-1}, representing 81.2%, 17.3% and 1.5% of the total oxidation capacity, respectively. For the suburban site, an average oxidation capacity of 2.43×10^7, 2.32×10^6 and 4.94×10^5 molecule cm^{-3} s^{-1} was calculated for OH, O_3 and NO_3 radicals,

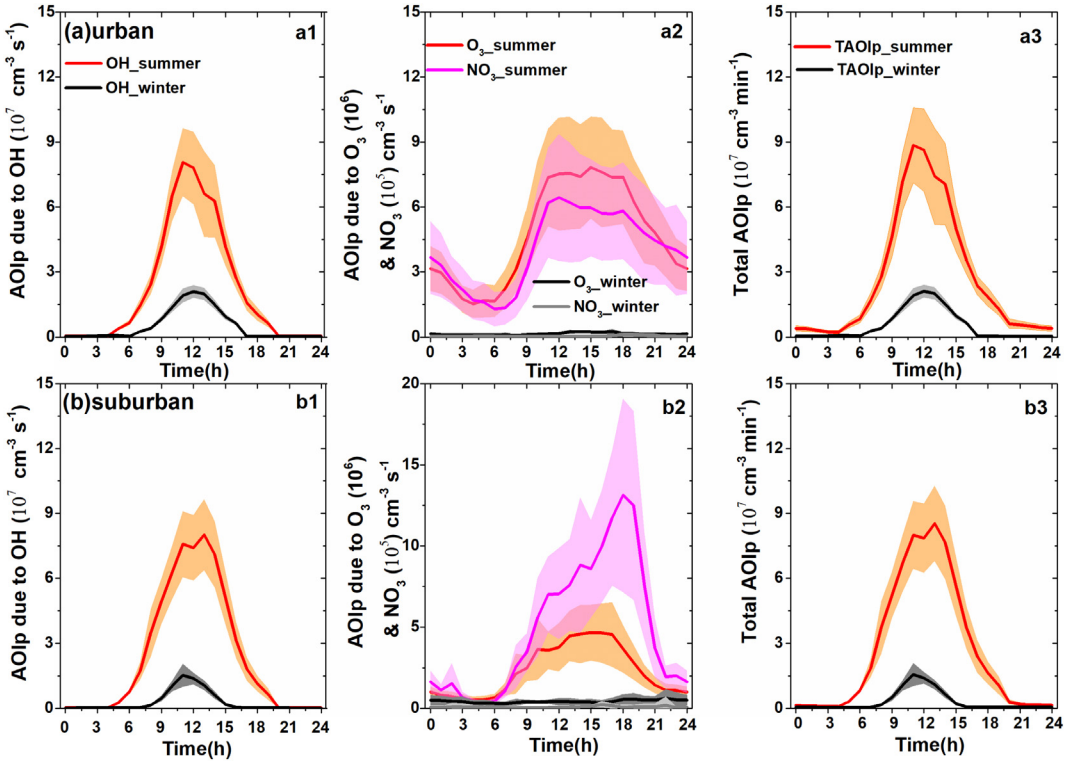

Fig. 5. Diurnal variation of AOIp due to three major oxidants (OH, O_3 and NO_3) and the total AOIp at the (a) urban and (b) suburban sites in Beijing during the summer and winter campaigns.

representing 89.6%, 8.6% and 1.8% of the total oxidation capacity, respectively. As expected, the dominant contributor to the AOIp during the daytime was OH, while O_3 was the second most important oxidant at both sites (Fig. 6a). The major fuels for O_3 oxidation at both sites were alkenes (>95%), while aromatics contributed the rest part. In comparison, NO_3 made minor contributions owing to the lower abundance of OVOCs (Table 1). During the winter campaign, the diurnal patterns of AOIp almost resembled those in summer, but with much lower peak values at the urban (2.11×10^7 molecule cm^{-3} s^{-1}) and suburban (1.56×10^7 molecule cm^{-3} s^{-1}) sites. Note that the peak value at the urban site appeared at 12:00, which was 1 h later than that in summer, while the peak value at the suburban site appeared 2 h earlier than that in summer. The average oxidation capacity of OH, O_3 and NO_3 radicals was approximately 10-fold lower than those in summer for both sites. Still, OH was the predominant contributor to the AOIp during daytime (Fig. 6a), with contributions of 97.3% and 89.4% to the total oxidation capacity for the urban and suburban sites, respectively. Ozone was the second most important oxidant, with contributions of 2.7% and 10.4%, which dominated the AOC during the nighttime (>60%) at both sites. Alkenes (96.8% for urban, 91.7% for suburban) were the dominate fuels for O_3 oxidation at both sites. Similar to summer, negligible contributions from NO_3 were observed for both sites owing to the relatively lower abundances of OVOCs. In general, OH dominated the AOC in the urban and suburban area of Beijing, which is consistent with previous studies in different urban locations (Elshorbany et al., 2009; Bannan et al., 2015; Xue et al., 2016; Zhu et al., 2020).

To specify the major reactant species consuming OH, the loss frequency of the different reactants to OH was determined using the indicator of OH reactivity (L_{OH}, Xue et al., 2016). During the summer campaign, the average values of L_{OH} were 23.92 ± 6.01 s^{-1} and 16.82 ± 7.32 s^{-1} for the urban and suburban sites, comparable with results reported in other megacities of China, which ranged from 15 s^{-1} to 30 s^{-1} (Tan et al., 2019). As shown in Fig. 7a, VOCs, CO and NO_2 were major contributors to OH reactivity in summer Beijing, which is consistent with previous studies (Ling et al., 2014; Zhu et al., 2020). Note that the contribution of VOCs to the total OH reactivity was higher at the urban site, which might be attributable to the different contributions of the VOCs group. Alkenes clearly dominated the OH reactivity at the suburban site (Fig. 7b), with maxima in the early morning and late afternoon (Fig. 6b); whereas, both alkenes and aromatics dominated the OH reactivity at the urban site during the daytime (Fig. 6b). The OH reactivity was slightly higher during wintertime at the urban site (27.79 ± 19.15 s^{-1}), covering a range from 3.4 to 113 s^{-1}, which is comparable with previous results observed in Paris during the 2010 MEGAPOLI winter campaign (10–130 s^{-1}; Dolgorouky et al., 2012), as well as observations in urban Beijing during pollution episodes (27 s^{-1}; Ma et al., 2019). Conversely, the winter OH reactivity at the suburban site increased significantly, with an average value of 52.58 ± 48.37 s^{-1}, which was much higher than that at the urban site and mainly attributable to the abnormally high levels of NO (up to 380 ppb) observed at the suburban site during the winter campaign (Fig. 1). The high levels of NO observed at the suburban site during wintertime possibly due to the emissions from heavy trucks, the intense biomass burning activity, and the "Coal to Gas" project as reported in a recent study (Zhao et al., 2020). As shown in Fig. 7a, the contribution of NO to the total OH reactivity was much higher at the suburban site (36.89%) than that at the urban site (25.98%). In comparison, the contribution of VOCs to the total OH reactivity was comparable at these two sites during wintertime, both of which were dominated by the alkenes (Fig. 7b), with maxima in the late afternoon (Fig. 6b). In addition, a higher contribution of OVOCs but lower contribution of aromatics to the total OH reactivity was observed at the urban site compared with

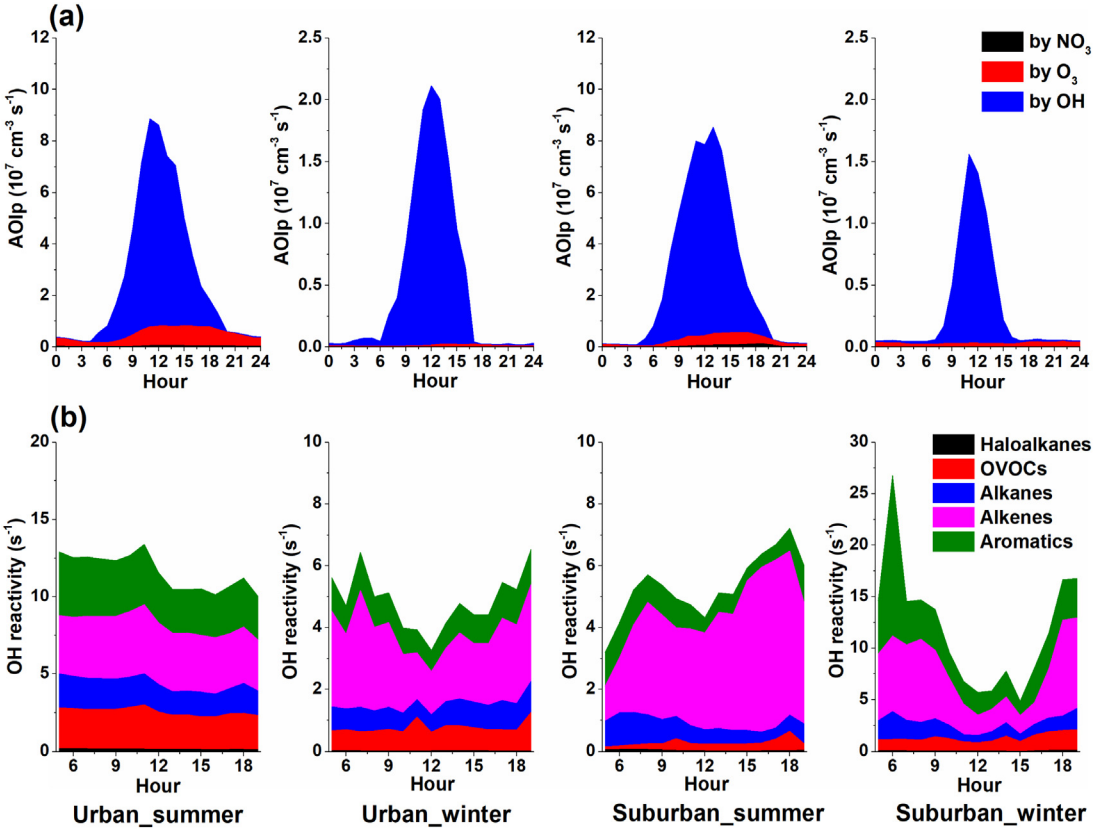

Fig. 6. (a) Contributions of major oxidants to the diurnal pattern of AOIp and (b) portioning of the daytime OH reactivity by oxidation of major VOC groups during summer and winter campaigns at the urban and suburban sites of Beijing.

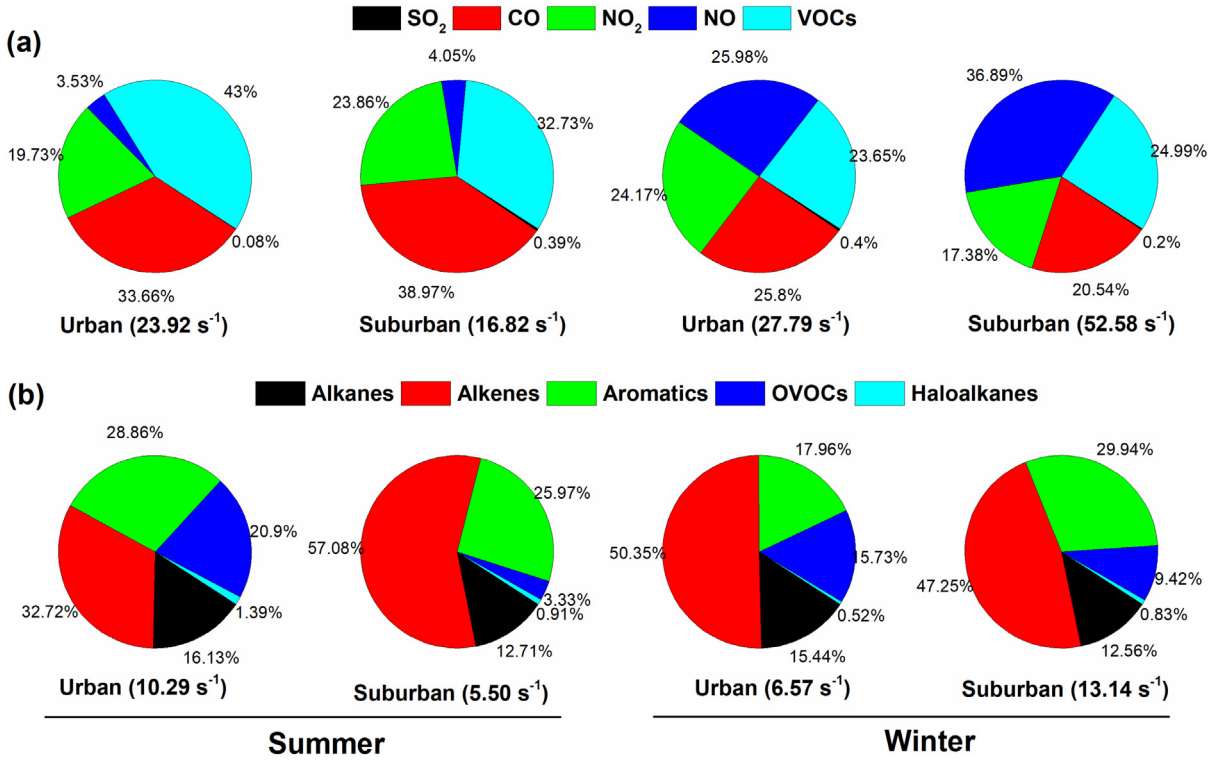

Fig. 7. (a) Average contributions of major groups of reactants to the total OH reactivity at the urban and suburban sites during the summer and winter campaigns. (b) Contribution of each VOC group to the OH reactivity of VOCs at the urban and suburban sites during the summer and winter campaigns.

those at the suburban site (Fig. 7b). These results are different to those observed in the Pearl River Delta region (Lou et al., 2010) and central London (Whalley et al., 2016), where alkenes and aromatics have been found to account for minor fractions and secondary OVOCs dominated the OH reactivity. This kind of discrepancy may have resulted in the different concentrations of VOC groups and might also be associated with the limited OVOC species measured in this study.

3.2.3. Comparison of AOIe and AOIp

As shown in Table 1, AOIe and AOIp presented different seasonal trends at both sites. Although reduced values in winter were apparent for both AOIe and AOIp, the magnitude of reduction was more significant for AOIp, especially at the suburban site. For example, the average reduction in AOIe from summer to winter was 40.9% and 12.7% for the urban and suburban sites, respectively, whereas for AOIp it was 81.8% and 88.5%. Note that the average winter AOIp at the suburban site decreased more obviously compared to that at the urban site, which was opposite to the seasonal trend of AOIe at these two sites (Table 1). In addition, the diurnal patterns of AOIe and AOIp were also distinct, especially during wintertime at both sites. While AOIe showed higher values at nighttime in winter (Fig. 3), a unimodal diurnal pattern with peak values at noon was evident for AOIp (Fig. 5). In general, AOIe and AOIp showed different seasonal variations and diurnal patterns at both sites, which suggests inconsistency between these two AOC indexes in qualifying the oxidative capacity of the atmosphere. By definition, AOIe denotes estimation of oxidative capacity based on the oxidation products, such as the major gaseous-phase and major particle-phase oxidation products, while AOIp denote the potential oxidative capacity based on the bi-molecular reaction between major reactants and major oxidants (OH, O_3 and NO_3). Thus, both AOIe and AOIp neglect the complex intermediate processes that convert the reactants into the final oxidation products. Since the oxidation products are formed from a variety of reaction processes, such as gas-phase reactions, liquid-phase reactions and heterogeneous reactions, the variations in AOIe should thus be close to the actual AOC. In addition, as AOIe highly depends on the concentrations of these secondary pollutants which are formed from both local transformation and regional transported and are relatively long lived, thus AOIe would be represent AOC more regionally. Conversely, only gas-phase reactions are considered in AOIp, which will underestimate the AOC in the absence of liquid-phase and heterogeneous reactions. In addition, some active VOC species, such as formaldehyde and acetaldehyde, were not measured in this study and thus may also introduce uncertainty in the calculation potential of AOC. Assuming AOIe represents the actual AOC, the sources of underestimation for AOIp are discussed in the following budget analysis.

3.3. Quantitative analysis of the AOC index methods

Both indexes are based on different time frames. AOIe is based on the past time frame, and describes the amount of electron transfer (representing secondary pollutant formation) during the oxidation history. In comparison, AOIp is a present time frame index, and describes the instantaneous reaction rates of a variety of primary reactants with major oxidants. Their units are also different, AOIe is a concentration, while AOIp is a reaction rate. As AOIe and AOIp are calculated from different datasets and they have different time frames and different dimensions, we concentrate on comparing the diurnal patterns of these two AOC indexes after they have been normalized to dimensionless values. The dimensionless procedure was based on the average diurnal variation data and normalized by dividing the maximum hourly value in each season. Note that the difference in the diurnal pattern of AOIe and AOIp could be attributed to the different transformation processes associated with them. As discussed in Section 3.2.3, AOIp was calculated based solely on gas-phase reactions (MCM), and could be represent the potential oxidizing capacity. In comparison, not only gas-phase reactions, but also liquid-phase reactions and heterogeneous reactions were included in AOIe as it was calculated from the oxidation products, which could be represent the apparent oxidizing capacity. Thus, the

comparison of AOIp and AOIe in diurnal pattern would be expected to explore whether the AOC is properly represented by current photochemical mechanism (e.g. MCM 3.3.1) or not. Fig. 8a and b show the diurnal variations of normalized AOIe and AOIp at the urban and suburban sites. During the summer campaign, AOIe and AOIp shared the same daytime peak at about 12:00. Clearly, there was underestimation of AOC by AOIp during the whole day, except at noon, at both sites. In particular, the maximum underestimation was at nighttime, ranging from 83% to 96% at the urban site and from 80% to 97% at the suburban site (Fig. 8a). In wintertime, underestimation of AOC by AOIp also prevailed at nighttime, ranging from 98% to 99% at the urban site and from 94% to 96% at the suburban site. The possible sources that contributed to the underestimation of AOIp are discussed.

3.3.1. Underestimation due to missing major secondary OVOCs

As shown in Fig. 7b, OVOCs contributed a minor fraction to the OH reactivity in this study, at about 4%–8% in the urban site, which is much lower than that reported in urban environments, ranging from 20% to 23% (Tan et al., 2019). Note that only 12 OVOCs were measured and included in the AOIp estimation, and other reactive OVOCs such as aldehydes and ketone were not measured thus would underestimation the contribution of OVOCs to AOIp. To evaluate the contribution of unmeasured OVOC species, we used a box model—Framework for 0-Dimensional Atmospheric Modeling (F0AM), based on MCM3.3.1, to simulate the ambient levels of OVOCs constrained by observations. Detail description about the F0AM model has been reported in our recent work (Liu et al., 2021) and a brief description was provided in the SI. A high-O_3 day during summertime (4 July 2018) and a high particle-loading day during wintertime (12 January 2019) were selected as case studies for the simulation of OVOCs at the urban site. The model results suggested that the AOC will be largely underestimated without the OVOC group. As shown in Fig. S5, aldehydes and ketone compounds contributed a considerable proportion of OH consumption when calculating the OH budget analysis. Among the aldehydes and ketones, formaldehyde, acetaldehyde and benzaldehyde were the three major fuels for which the consumption rate of OH contributed by them could reach up to 10 ppb/h, accounting for nearly 30% of the total consumption rate of OH. In comparison, the contributions of these three OVOC species to OH consumption in winter were relatively low (Fig. 7b), with a consumption rate of OH at about 2 ppb/h, accounting for about 12% of the total consumption rate of OH. Thus, the simulated OVOC species were included in the AOIp calculation to minimize the underestimation of AOC.

3.3.2. Underestimation due to the missing heterogeneous mechanism

Current air quality models are unable to reproduce the extremely high concentrations of fine particles during heavy haze episodes, which is mainly attributed to underestimation of secondary aerosols such as sulfate owing to the lack of a heterogeneous mechanism (Shao et al., 2019). This suggests that the AOC will be largely underestimated if the heterogeneous mechanism is not considered, which was confirmed by the comparison of AOIp to AOIe in this study. To evaluate the contribution of heterogeneous processes to the AOC, we used a multiphase chemical box model (RACM-CAPRAM) constrained by observations to elucidate the heterogeneous mechanism in the formation of sulfate and nitrate. Detail description about the RACM-CAPRAM model has been reported in previous work (Wen et al., 2018) and a brief description was provided in the SI. Note that heterogeneous sulfate production, which refers to aqueous phase oxidation of S(IV) ($SO_2 \cdot H_2O + HSO_3^- + SO_3^{2-}$) on the surface of and/or within the bulk preexisting aerosols were also considered and four heterogeneous sulfate production mechanisms (via H_2O_2, O_3, NO_2, and TMIs) on aerosols were coupled into the RACM-CAPRAM model. More details on the heterogeneous sulfate production mechanisms were briefly present in the SI and could be also found in Shao et al. (2019).

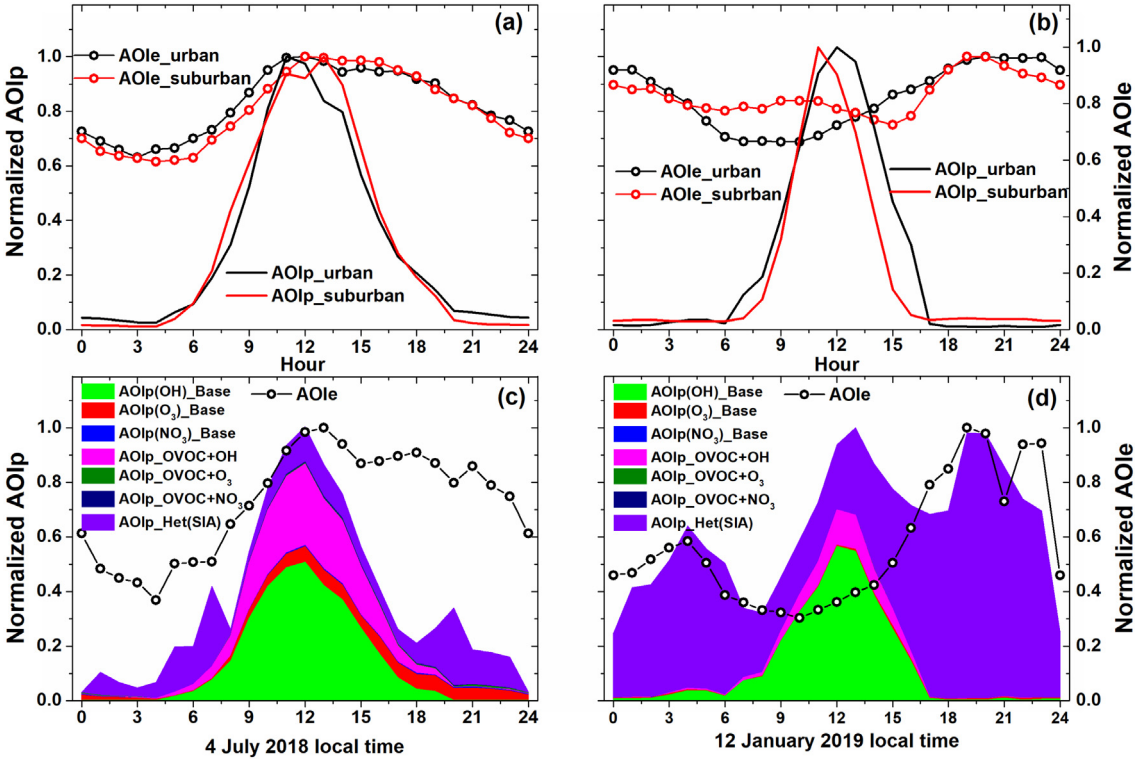

Fig. 8. Diurnal variation of normalized AOIe and AOIp during the (a) summer campaign and (b) winter campaign, and improvement in the underestimation of AOIp by adding the modelled reaction of OVOCs with major oxidants and modelled heterogeneous reaction pathways of SIA (sulfate and nitrate) in (c) the summer case (4 July 2018) and (d) the winter case (12 January 2019).

To be consistent with the OVOC modelling results, the same summer case (4 July 2018) and winter case (12 January 2019) for the urban site were selected. As can be seen from Fig. S7, the contribution of the gas-phase homogeneous reaction only accounted for about 45% of sulfate enhancement in the winter case, while the contribution of the heterogeneous reaction exceeded 50% and dominated the sulfate production, which confirmed the underestimation of AOC if the heterogeneous mechanism is not considered. As for nitrate formation, the gas-phase homogeneous reaction contributed more than 95% of the nitrate increment, while the hydrolysis of N_2O_5 contributed more than 5% in the peak pollution stage. Therefore, the heterogeneous process of secondary inorganic aerosol (SIA) formation was further considered in the calculation of AOIp.

3.3.3. Improved AOIp in qualifying AOC

Based on the above analysis, the modelled OVOC species and the heterogeneous process of SIA formation were included in the AOIp calculation, and the normalized results were then compared with the normalized AOIe for the case studies. Fig. 8c and d show the improved AOIp for the summer and winter cases. As shown in Fig. 8c, the added OVOCs contributed a large fraction to the total AOIp in the summer case, with an average contribution of 25.7% during the daytime, which was significantly higher than that when only the nine kinds of OVOC species measured in this study were considered (5.8%). In addition, OH dominated the added contribution of OVOCs, especially during the daytime. Furthermore, the contribution of OVOCs to the OH reactivity was increased to 37.1% when the modelled OVOC species were included, which is comparable to previous studies (20%–60%) conducted in urban environments during summertime (Xue et al., 2016; Li et al., 2018; Tan et al., 2019). Note that a considerable contribution from the heterogeneous oxidation of SO_2 and NO_2 (27.4%) was observed, especially during the nighttime and early morning, with the maximum contribution of 85.6% at about 04:00. As a result, the underestimation of AOIp during the summer case improved substantially, ranging from 56% to 93%. Different to the summer case, the added OVOCs only contributed a minor fraction (2.9%) to the total AOIp, whereas the added AOIp was mainly attributable to the heterogeneous process of SIA formation. As shown in Fig. 8d, heterogeneous oxidation dominated AOIp at nighttime, and the variation of was consistent with AOIe at night. Consequently, the significantly underestimated AOIp at nighttime in winter was notably improved owing to the inclusion of heterogeneous oxidation in the AOIp calculation. Note that reminding large discrepancy between AOIe and AOIp at nighttime (Fig. 8) maybe also due to the overestimation of AOIe that contributed to the residual background and transport of secondary compounds.

Overall, the added OVOC species and heterogeneous oxidation processes in the calculation of AOIp largely improved the underestimation of AOIp in qualifying the AOC. However, it should be noted that discrepancies between AOIp and AOIe still exist, which may be attributable to the underestimation or overestimation of the parameterized radical concentrations, the missing of heterogeneous oxidation processes in the formation of SOA that are not yet considered in AOIp and the transported of secondary compounds that resulted in the overestimation of AOIe, which need to be further evaluated in future studies.

3.4. Implication for the air pollution formation

Atmospheric oxidation capacity (AOC) is important in estimating the occurrence of air pollution. As discussed above, the atmospheric oxidation capacity could be properly qualified by AOIe and AOIp, although the latter underestimated AOC in some extent during nighttime. To explore the relationship between these two AOC indexes and air quality, the distribution of AOIp and AOIe under different air pollution levels (Excellent: hourly $PM_{2.5} \leq 35$ μg/m^3; Good: 35 < hourly $PM_{2.5} \leq 75$ μg/m^3; Lightly polluted: 75 < hourly $PM_{2.5} \leq 115$ μg/m^3; Moderately/heavily polluted: hourly $PM_{2.5} > 115$ μg/m^3) were analyzed during the summer and winter campaigns (Fig. 9). As showed in Fig. 9a, continuous increase of AOIp was observed during summertime as the pollution level evolved from excellent to lightly polluted. When the air pollution further developed to moderately/heavily polluted, however, the average value of AOIp

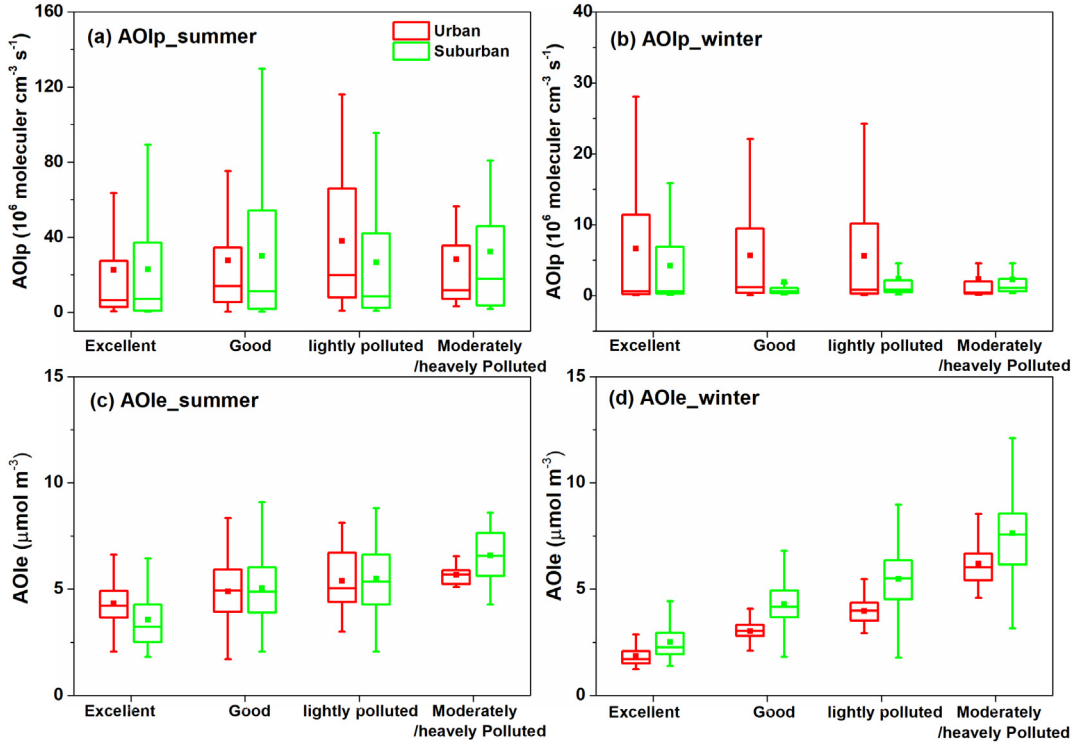

Fig. 9. The distribution of (a, b) AOIp and (c, d) AOIe under different air pollution levels (Excellent: hourly $PM_{2.5} \leq 35$ μg/m^3; Good: 35 < hourly $PM_{2.5} \leq 75$ μg/m^3; Lightly polluted: 75 < hourly $PM_{2.5} \leq 115$ μg/m^3; Moderately/heavily polluted: hourly $PM_{2.5} > 115$ μg/m^3) during the summer and winter campaigns. The whisker plot provides the 90th, 75th, 50th, 25th and 10th percentiles of the AOC index data.

showed a decrease trend. This kind of behavior for summer AOIp was different from summer AOIe, which showed a continuous increase trend when air pollution level evolved from excellent to moderately/heavily polluted conditions (Fig. 9c). Note that the evolution patterns were completely different for AOIp and AOIe during wintertime. While AOIp showed a decrease trend as air quality worsened, higher values of AOIe were observed under winter server pollution levels (Fig. 9d), consistent with that in summer. These results suggested AOIp was inadequate for the prediction of air pollution formation. At the same time, the evolution pattern of AOIe suggested atmospheric oxidation capacity was enhanced during heavy pollution episodes, which indicated the rapid increase of fine particles was most possibility mainly contributed by the intense secondary transformation of gaseous pollutants under enhanced AOC during pollution episodes. In fact, the observed fine particle chemical compositions during also support the above hypothesis, our long observations in fine particle chemical composition in urban Beijing (L. Liu et al., 2019; Z. Liu et al., 2019) and many previous studies conducted in other cities (Elser et al., 2016; Xie et al., 2019; Sun et al., 2019) all reported an increase contribution of secondary aerosol as air pollution developed from the clean stage to the heavily polluted stage. Furthermore, the decreased values of AOIp in polluted days may suggest that the current photochemical mechanism (e.g. MCM) could not properly represent the actual atmospheric oxidation capacity, especially for the wintertime. Our recent work suggested significantly underestimated of OH oxidation rates during wintertime when HONO heterogeneous sources was not considered in current MCM (Liu et al., 2021), which would be partly explained the underestimation of AOC by MCM during heavy pollution episodes. Overall, the newly developed AOC index (AOIe) well reflects the evolution of air pollution and could be used to air quality administration. Whereas, the AOIp index which based solely on gas-phase reactions largely underestimate AOC, especially during wintertime. Thus, our results highlight the urgent need to incorporate the heterogeneous mechanism with the photochemical mechanism to better qualify the atmospheric oxidation capacity.

4. Conclusion

To better understand the key processes governing the chemistry of the polluted urban atmosphere of northern China, we present a first detailed evaluation of atmospheric oxidation capacity (AOC) by using newly developed indexes (AOIe and AOIp), which were created and evaluated by a comprehensive suite of data taken from summer and winter field campaigns conducted in parallel at an urban and suburban site in Beijing from 1 June to 15 July 2018 and from 1 December 2018 to 15 January 2019, respectively.

The AOC showed a clear seasonal pattern, with stronger intensity in summer compared to winter. The gaseous-phase oxidation products (O_3 and NO_2) dominated the AOIe (~80%) during summertime at both sites, while the contribution of particle-phase oxidation products (sulfate, nitrate and secondary organic aerosol) to AOIe increased in winter (~30%). As for AOIp in summer, the dominant contributor at the urban site was alkenes (29.0%), while it was CO (35.5%) at the suburban site. Furthermore, it was mainly contributed by CO, NO_2 and NO at both sites during wintertime, accounting for 73.3% (urban) and 63.3% (suburban) of the total AOIp. As expected, the dominant oxidant that contributed to the AOIp during the daytime was OH, while O_3 was the second most important oxidant at both sites. During summertime, alkenes clearly dominated the OH reactivity at the suburban site, with maxima in the early morning and late afternoon; whereas, both alkenes and aromatics dominated the OH reactivity at the urban site during the daytime. The OH reactivity was higher during wintertime, which was dominated by the alkenes among the VOC species at both sites.

AOIe and AOIp presented different seasonal trends at both sites. Although the reduced values in winter were evident for both AOIe and AOIp, the magnitude of reduction was more significant for AOIp, especially at the suburban site. As AOIe and AOIp are calculated from different datasets and have different dimensions, the diurnal variations of normalized AOIe and AOIp were examined, which shared the same daytime peak but showed significant bias at nighttime. To explore the possible sources of deviation between AOIe and AOIp, a constrained photochemical box model based on the MCM (Master Chemical Mechanism) and a constrained multiphase chemical box model (RACM-CAPRAM) were used to evaluate AOC budgets and their source apportionment. Results suggested that unmeasured OVOC species and missed heterogeneous oxidation processes in the calculation of AOIp contributed substantially to the underestimation of AOC by AOIp, which should be taken into consideration in future AOC studies. In addition, discrepancy between AOIp and AOIe still existed after the addition of OVOCs and inclusions of heterogeneous oxidation processes, which may be attributable to the heterogeneous oxidation processes in the formation of SOA that are not yet considered in AOIp, which needs to be evaluated in future work. Overall, the newly developed AOC index (AOIe) well reflects the evolution of air pollution and could be used to air quality administration. Whereas, the underestimation of AOC by AOIp index highlight the urgent need to incorporate the heterogeneous mechanism with the photochemical mechanism to better qualify the atmospheric oxidation capacity.

CRediT authorship contribution statement

ZR, KD, YS and YH designed the experiments, and YD, YY, WK and XP carried out the field measurements and data analysis. ZR, JY and YZ performed the box model simulation. ZR and YS interpreted the data and wrote the paper. All the authors contributed to discussing results and commenting on the paper.

Declaration of competing interest

The authors declare that they have no competing interests.

Acknowledgement

This study was supported by the Ministry of Science and Technology of the People's Republic of China (Grant no. 2017YFC0210000), the Young Talent Project of the Center for Excellence in Regional Atmospheric Environment, CAS (CERAE202002), the National Natural Science Foundation of China (Grant no. 41705110), Beijing Municipal Natural Science Foundation (8192045) and Beijing Major Science and Technology Project (Z181100005418014). We would like to thank Prof. Likun Xue of Shandong University for the suggestion in calculation of AOC index, and thank the three anonymous referees for the constructive comments and suggestions. The authors also acknowledge all staff and workers participate in the field observations.

Data availability

All data in this study are available upon request to the corresponding authors.

Appendix A. Supplementary data

Supplementary data to this article can be found online at https://doi.org/10.1016/j.scitotenv.2021.145306.

References

Bannan, T.J., Booth, A.M., Bacak, A., Muller, J.B.A., Leather, K.E., Breton, M.L., Jones, B., Young, D., Coe, H., Allan, J., Visser, S., Slowik, J.G., Furger, M., Prévôt, A.S.H., Lee, J., Dunmore, R.E., Hopkins, J.R., Hamilton, J.F., Lewis, A.C., Whalley, L.K., Sharp, T., Stone, D., Heard, D.E., Fleming, Z.L., Leigh, R., Shallcross, D.E., Percival, C.J., 2015. The first UK measurements of nitryl chloride using a chemical ionization mass spectrometer in central London in the summer of 2012, and an investigation of the role of Cl atom oxidation. J. Geophys. Res.-Atmos. 120, 5638–5657.

Chan, C.K., Yao, X., 2008. Air pollution in mega cities in China. Atmos. Environ. 42, 1–42. https://doi.org/10.1016/j.atmosenv.2007.09.003.

Dolgorouky, C., Gros, V., Sarda-Esteve, R., Sinha, V., Williams, J., Marchand, N., Sauvage, S., Poulain, L., Sciare, J., Bonsang, B., 2012. Total OH reactivity measurements in Paris during the 2010 MEGAPOLI winter campaign. Atmos. Chem. Phys. 12, 9593–9612.

Ehhalt, D.H., Rohrer, F., 2000. Dependence of the OH concentration on solar UV. J. Geophys. Res. Atmos. 105 (D3), 3565–3571.

Elser, M., Huang, R.J., Wolf, R., Slowik, J.G., Wang, Q.Y., Canonaco, F., Li, G.H., Bozzetti, C., Daellenbach, K.R., Huang, Y., Zhang, R.J., Li, Z.Q., Cao, J.J., Baltensperger, U., El-Haddad, I., Prevot, A.S.H., 2016. New insights into $PM_{2.5}$ chemical composition and sources in two major cities in China during extreme haze events using aerosol mass spectrometry. Atmos. Chem. Phys. 16, 3207–3225.

Elshorbany, Y.F., Kurtenbach, R., Wiesen, P., Lissi, E., Rubio, M., Villena, G., Gramsch, E., Rickard, A.R., Pilling, M.J., Kleffmann, J., 2009. Oxidation capacity of the city air of Santiago, Chile. Atmos. Chem. Phys. 9, 2257–2273. https://doi.org/10.5194/acp-9-2257-2009.

Gao, M., Guttikund, S.K., Carmichael, G.R., Wang, Y., Liu, Z., Stanier, C.O., Saide, P.E., Yu, M., 2015. Health impacts and economic losses assessment of the 2013 severe haze event in Beijing area. Sci. Total Environ. 511, 553–561.

Gao, M., Liu, Z., Zheng, B., et al., 2020. China's emission control strategies have suppressed unfavorable influences of climate on wintertime $PM_{2.5}$ concentrations in Beijing since 2002. Atmos. Chem. Phys. 20, 1497–1505.

George, C., Strekowski, R.S., Kleffmann, J., Stemmler, K., Ammann, M., 2005. Photoenhanced uptake of gaseous NO_2 on solid organic compounds: a photochemical source of HONO? Faraday Discuss. 130, 195–210.

Geyer, A., Alicke, B., Konrad, S., Schmitz, T., Stutz, J., Platt, U., 2001. Chemistry and oxidation capacity of the nitrate radical in the continental boundary layer near Berlin. J. Geophys. Res. 106, 8013–8025.

Li, Z., Xue, L., Yang, X., Zha, Q., Tham, Y., Yan, Chao, Louie, P.K.K., Luk, W.Y.C., Wang, T., Wanga, W., 2018. Oxidizing capacity of the rural atmosphere in Hong Kong, Southern China. Sci. Total Environ. 612, 1114–1122.

Li, K., Jacob, D.J., Liao, H., Shen, L., Zhang, Q., Bates, K.H., 2019. Anthropogenic drivers of 2013–2017 trends in summer surface ozone in China. Proc. Natl. Acad. Sci. U.S.A. 116, 422–427. https://doi.org/10.1073/pnas.1812168116.

Li, J., Liu, Z., Cao, L., Gao, W., Yan, Y., Mao, J., Zhang, X., He, L., Xin, J., Tang, G., Ji, D., Hu, B., Wang, L., Wang, Y., Dai, L., Zhao, D., Du, W., Wang, Y., 2020a. Highly time-resolved chemical characterization and implications of regional transport for submicron aerosols in the North China Plain. Sci. Total Environ., 135803 https://doi.org/10.1016/j.scitotenv.2019.135803.

Li, J., Liu, Z., Gao, W., Tang, G., Hu, B., Ma, Z., Wang, Y., 2020b. Insight into the formation and evolution of secondary organic aerosol in the megacity of Beijing, China. Atmos. Environ. 220, 117070.

Ling, Z.H., Guo, H., Lam, S.H.M., Saunders, S.M., Wang, T., 2014. Atmospheric photochemical reactivity and ozone production at two sites in Hong Kong: application of a master chemical mechanism-photochemical box model. J. Geophys. Res.-Atmos. 119, 10567–10582. https://doi.org/10.1002/2014jd021794.

Liu, Z., Hu, B., Wang, L., Wu, F., Gao, W., Wang, Y., 2015. Seasonal and diurnal variation in particulate matter (Pm10 and pm25) at an urban site of Beijing: analyses from a 9-year study. Environ. Sci. Pollut. Res. 22 (1), 627–642. https://doi.org/10.1007/s11356-014-3347-0.

Liu, Z., Hu, B., Zhang, J., Yu, Y., Wang, Y., 2016. Characteristics of aerosol size distributions and chemical compositions during wintertime pollution episodes in Beijing. Atmos. Res. 168, 1–12. https://doi.org/10.1016/j.atmosres.2015.08.013.

Liu, Z., Gao, W., Yu, Y., Hu, B., Xin, J., Sun, Y., Wang, L., Wang, G., Bi, X., Zhang, G., et al., 2018. Characteristics of $PM_{2.5}$ mass concentrations and chemical species in urban and background areas of China: emerging results from the CARE-China network. Atmos. Chem. Phys. 18, 8849–8871.

Liu, L., Bei, N., Wu, J., et al., 2019a. Effects of stabilized Criegee intermediates (sCIs) on sulfate formation: a sensitivity analysis during summertime in Beijing–Tianjin–Hebei (BTH), China. Atmos. Chem. Phys. 19, 13341–13354.

Liu, Z., Hu, B., Ji, D., Cheng, M., Gao, W., Shi, S., Xie, Y., Yang, S., Gao, M., Fu, H., Chen, J., Wang, Y., 2019b. Characteristics of fine particle explosive growth events in Beijing, China: seasonal variation, chemical evolution pattern and formation mechanism. Sci. Total Environ. 687, 1073–1086. https://doi.org/10.1016/j.scitotenv.2019.06.068.

Liu, J., Liu, Z., Ma, Z., Yang, S., Yao, D., Zhao, S., Hu, B., Tang, G., Sun, J., Cheng, M., Xu, Z., Wang, Y., 2021. Detailed budget analysis of HONO in Beijing, China: implication on atmosphere oxidation capacity in polluted megacity. Atmos. Environ. 244, 117957.

Lou, S., Holland, F., Rohrer, F., Lu, K., Bohn, B., Brauers, T., Chang, C.C., Fuchs, H., Häseler, R., Kita, K., Kondo, Y., Li, X., Shao, M., Zeng, L., Wahner, A., Zhang, Y., Wang, W., Hofzumahaus, A., 2010. Atmospheric OH reactivities in the Pearl River Delta – China in summer 2006: measurement and model results. Atmos. Chem. Phys. 10, 11243–11260. https://doi.org/10.5194/acp-10-11243-2010.

Lu, K.D., Rohrer, F., Holland, F., Fuchs, H., Bohn, B., Brauers, T., Chang, C.C., Häseler, R., Hu, M., Kita, K., Kondo, Y., Li, X., Lou, S.R., Nehr, S., Shao, M., Zeng, L.M., Wahner, A., Zhang, Y.H., Hofzumahaus, A., 2012. Observation and modelling of OH and HO_2 concentrations in the Pearl River Delta 2006: a missing OH source in a VOC rich atmosphere. Atmos. Chem. Phys. 12, 1541–1569. https://doi.org/10.5194/acp-12-1541-2012.

Lu, K., Guo, S., Tan, Z., Wang, H., Shang, D., Liu, Y., Li, X., Wu, Z., Hu, M., Zhang, Y., 2018. Exploring atmospheric free-radical chemistry in China: the self-cleansing capacity and the formation of secondary air pollution. Natl. Sci. Rev. 0, 1–16. https://doi.org/10.1093/nsr/nwy073.

Ma, X., Tan, Z., Lu, K., et al., 2019. Winter photochemistry in Beijing: observation and model simulation of OH and HO_2 radicals at an urban site. Sci. Total Environ. 685, 85–95.

Parrish, D.D., Singh, H.B., Molina, L., Madronich, S., 2011. Air quality progress in North American megacities: a review. Atmos. Environ. 45, 7015–7025. https://doi.org/10.1016/j.atmos env.2011.09.039.

Prinn, G.R., 2003. The cleansing capacity of the atmosphere. Annu. Rev. Environ. Resour. 28 (29–57) 2001.

Shao, J., Chen, Q., Wang, Y., Lu, X., He, P., Sun, Y., Shah, V., Martin, R.V., Philip, S., Song, S., Zhao, Y., Xie, Z., Zhang, L., Alexander, B., 2019. Heterogeneous sulfate aerosol formation mechanisms during wintertime Chinese haze events: air quality model assessment using observations of sulfate oxygen isotopes in Beijing. Atmos. Chem. Phys. 19, 6107–6123.

Stemmler, K., Ammann, M., Dondors, C., Kleffmann, J., George, C., 2006. Photosensitized reduction of nitrogen dioxide on humic acid as a source of nitrous acid. Nature 440, 195–198.

Stemmler, K., Ndour, M., Elshorbany, Y., Kleffmann, J., D'Anna, B., George, C., Bohn, B., Ammann, M., 2007. Light induced conversion of nitrogen dioxide into nitrous acid on submicron humic acid aerosol. Atmos. Chem. Phys. 7, 4237–4248. http://www.atmos-chem-phys.net/7/4237/2007/.

Sun, W., Wang, D., Yao, L., Fu, H., Fu, Q., Wang, H., Li, Q., Wang, L., Yang, X., Xian, A., Wang, G., Xiao, H., Chen, J., 2019. Chemistry-triggered events of $PM_{2.5}$ explosive growth during late autumn and winter in Shanghai, China. Environ. Pollut. 254, 112864.

Tan, Z., Lu, K., Jiang, M., Su, R., Wang, H., Lou, S., Fu, Q., Zhai, C., Tan, Q., Yue, D., Chen, D., Wang, Z., Xie, S., Zeng, L., Zhang, Y., 2019. Daytime atmospheric oxidation capacity in four Chinese megacities during the photochemically polluted season: a case study based on box model simulation. Atmos. Chem. Phys. 19, 3493–3513. https://doi.org/10.5194/acp-19-3493-2019.

Tham, Y.J., Wang, Z., Li, Q., Wang, W., Wang, X., Lu, K., Ma, N., Yan, C., Kecorius, S., Wiedensohler, A., Zhang, Y., Wang, T., 2018. Heterogeneous N_2O_5 uptake coefficient and production yield of $ClNO_2$ in polluted northern China: roles of aerosol water content and chemical composition. Atmos. Chem. Phys. 18, 13155–13171. https://doi.org/10.5194/acp-18-13155-2018.

Wang, Y., Yao, L., Wang, L., Liu, Z., Ji, D., Tang, G., Zhang, J., Sun, Y., Hu, B., Xin, J., 2014a. Mechanism for the formation of the January 2013 heavy haze pollution episode over central and eastern China. Sci. China Earth Sci. 57 (1), 14–25.

Wang, Y., Zhang, Q., Jiang, J., Zhou, W., Wang, B., He, K., Duan, F., Zhang, Q., Philip, S., Xie, Y., 2014b. Enhanced sulfate formation during China's severe winter haze episode in January 2013 missing from current models. J. Geophys. Res.-Atmos. 119, 10425–10440. https://doi.org/10.1002/2013jd021426.

Wang, M., Zeng, L., Lu, S., Shao, M., Liu, X., Yu, X., Chen, W., Yuan, B., Zhang, Q., Hu, M., Zhang, Z., 2014c. Development and validation of a cryogen-free automatic gas chromatograph system (GC-MS/FID) for online measurements of volatile organic compounds. Anal. Methods 6, 9424–9434.

Wang, Y., Li, W., Gao, W., Liu, Z., Tian, S., Shen, R., Ji, D., Wang, S., Wang, L., Tang, G., Song, T., Cheng, M., Wang, G., Gong, Z., Hao, J., Zhang, Y., 2019. Trends in particulate matter and its chemical compositions in China from 2013–2017. Sci. China Earth Sci. 62. https://doi.org/10.1007/s11430-018-9373-1.

Wang, Y., Gao, W., Wang, S., et al., 2020. Contrasting trends of $PM_{2.5}$ and surface-ozone concentrations in China from 2013 to 2017. Natl. Sci. Rev., nwaa032 https://doi.org/10.1093/nsr/nwaa032.

Wen, L., Xue, L., Wang, X., Xu, C., Chen, T., Yang, L., Wang, T., Zhang, Q., Wang, W., 2018. Summertime fine particulate nitrate pollution in the North China Plain: increasing trends, formation mechanisms and implications for control policy. Atmos. Chem. Phys. 18, 11261–11275.

Whalley, L.K., Stone, D., Bandy, B., Dunmore, R., Hamilton, J.F., Hopkins, J., Lee, J.D., Lewis, A.C., Heard, D.E., 2016. Atmospheric OH reactivity in central London: observations, model predictions and estimates of in situ ozone production. Atmos. Chem. Phys. 16, 2109–2122. https://doi.org/10.5194/acp-16-2109-2016.

Xie, Y., Liu, Z.R., Wen, T., Huang, X., Liu, J., Tang, G., Yang, Y., Li, X., Shen, R., Hu, B., Wang, Y., 2019. Characteristics of chemical composition and seasonal variations of $PM_{2.5}$ in Shijiazhuang, China: impact of primary emissions and secondary formation. Sci. Total Environ. 677, 215–229.

Xue, L., Gu, R., Wang, T., Wang, X., Saunders, S., Blake, D., Louie, P.K.K., Luk, C.W.Y., Simpson, I., Xu, Z., Wang, Z., Gao, Y., Lee, S., Mellouki, A., Wang, W., 2016. Oxidative capacity and radical chemistry in the polluted atmosphere of Hong Kong and Pearl River Delta region: analysis of a severe photochemical smog episode. Atmos. Chem. Phys. 16, 9891–9903. https://doi.org/10.5194/acp-16-9891-2016.

Yang, Y., Ji, D., Sun, J., Wang, Y., Yao, D., Zhao, S., Yu, X., Zeng, L., Zhang, R., Zhang, H., Wang, Y., Wang, Y., 2019. Ambient volatile organic compounds in a suburban site between Beijing and Tianjin: concentration levels, source apportionment and health risk assessment. Sci. Total Environ. 695, 133889.

Yuan, B., Hu, W.W., Shao, M., Wang, M., Chen, W.T., Lu, S.H., Zeng, L.M., Hu, M., 2013. VOC emissions, evolutions and contributions to SOA formation at a receptor site in eastern China. Atmos. Chem. Phys. 13, 8815–8832. https://doi.org/10.5194/acp-13-8815-2013.

Zhang, L., Liu, L., Zhao, Y., Gong, S., Zhang, X., Henze, D.K., Capps, S.L., Fu, T.M., Zhang, Q., Wang, Y., 2015. Source attribution of particulate matter pollution over North China with the adjoint method. Environ. Res. Lett. 10, 084011.

Zhang, Q., Zheng, Y., Tong, D., et al., 2019. Drivers of improved $PM_{2.5}$ air quality in China from 2013 to 2017. Proc. Natl. Acad. Sci. U.S.A. 116 (49), 24463–24469. www.pnas.org/cgi/doi/10.1073/pnas.1907956116.

Zhao, S., Hu, B., Gao, W., et al., 2020. Effect of the "coal to gas" project on atmospheric NOX during the heating period at a suburban site between Beijing and Tianjin. Atmos. Res. 241, 104977.

Zheng, J., Hu, M., Zhang, R., Yue, D., Wang, Z., Guo, S., Li, X., Bohn, B., Shao, M., He, L., Huang, X., Wiedensohler, A., Zhu, T., 2011. Measurements of gaseous H2SO4 by AP-ID-CIMS during CAREBeijing 2008 Campaign. Atmos. Chem. Phys. 11, 7755–7765. https://doi.org/10.5194/acp-11-7755-2011.

Zheng, B., Zhang, Q., Zhang, Y., He, K.B., Wang, K., Zheng, G.J., Duan, F.K., Ma, Y.L., Kimoto, T., 2015. Heterogeneous chemistry: a mechanism missing in current models to explain secondary inorganic aerosol formation during the January 2013 haze episode in North China. Atmos. Chem. Phys. 15, 2031–2049. https://doi.org/10.5194/acp-15-2031-2015.

Zhu, J., Wang, S., Wang, H., Jing, S., Lou, S., Saiz-Lopez, A., Zhou, B., 2020. Observationally constrained modeling of atmospheric oxidation capacity and photochemical reactivity in Shanghai, China. Atmos. Chem. Phys. 20, 1217–1232.